Journal of Power Sources, 48 (1994) 179–193

Effect of corrosion layer on phenomena that cause premature capacity loss in lead/acid batteries

D. Pavlov

Central Laboratory of Electrochemical Power Sources, Bulgarian Academy of Sciences, Sofia 1113 (Bulgaria)

Abstract

An analysis is given of the results presented in a number of studies of the phenomena that cause premature capacity loss (PCL). The work is reviewed in relation to the gel–crystal concept of the structure of the corrosion layer (CL) and the active mass. Using a specially designed plate with lead and lead–antimony sub-grids, it has been found that the phenomena leading to PCL proceed in the CL and at its interface with the positive active mass (PAM). The gel–crystal structure of this interface is discussed. The effects of PAM density, tin and antimony content in the grid alloy, and $PbSO_4$ content in the corrosion layer, on plate capacity have been investigated using specially designed tubular powder electrodes. It is established that a CL with appropriate properties can be formed during the curing procedure if the process is conducted at high temperatures. The outer, porous, corrosion sublayer and its interface with the PAM both consist of crystal and gel zones. The electric conductivity of gel zones is lower than that of crystal zones and depends on the concentration of polymer chains in the gel, and on the contact between them. On cycling, the concentration of polymer chains is decreased. This gives rise to decrease in the electric conductivity of the CL/PAM interface (the most critical element in the plate) and, consequently, to decline in plane capacity. Antimony and tin ions interconnect the polymer chains into an integral network that maintains a high concentration of polymer chains and, hence, a high electric conductivity of the CL/PAM interface. In this way, the phenomena that promote PCL are suppressed. The same effect is also achieved by increasing the density of the PAM and/or restricting mechanically the pulsations of the positive-plate volume during charge/discharge cycling.

Definition of 'premature capacity loss'

Choosing a name for the phenomena

In 1881, Sellon substituted the pure-lead grids of lead/acid battery plates with grids made from lead–antimony (6 to 12 wt.%Sb) alloys. The purpose of this change was to improve both the mechanical and the casting properties of the grids. It transpired, however, that antimony accelerated the decomposition of water. To reduce the maintenance of stationary batteries, the Bell Telephone Co., during the 1930s, substituted lead–antimony battery grids with lead–calcium ones [1]. It subsequently observed that the battery life was considerably shortened on deep-discharge cycling (Fig. 1).

Investigations have demonstrated that the above effect is due to the absence of antimony, rather than to the presence of calcium [2]. That is why this phenomenon was, at first, called the 'antimony-free-effect' (AFE). The term is based historically on the assumption that the reference capacity/cycle-life curve is that of plates with high-antimony lead–alloy grids.

SSDI 0378-7753(93)01865-F

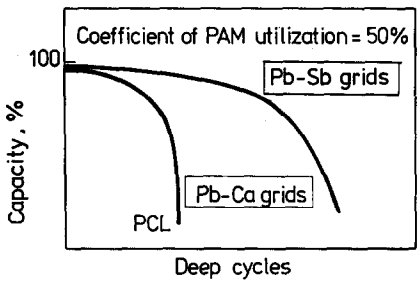

Fig. 1. Capacity of batteries with lead–calcium and high-antimony lead alloy grids on cycling; a demonstration of the early capacity decline of batteries; PCL: premature capacity loss.

Later, it was established that batteries with low-antimony grids also exhibit reduced cycle lives. Therefore, to make the definition of the phenomenon more precise, 'antimony' was excluded from its name and it was termed 'early capacity loss' (ECL), or 'premature capacity loss' (PCL), or 'relaxable insufficient mass utilization' (RIMU). At present, the term 'premature capacity loss' appears to have gained popularity in the literature.

The question arises, then, whether it is not more logical to take the capacity/cycle-life curve of batteries with pure-lead grids as the benchmark. In this case, the behaviour of batteries with lead-alloy grids (tin, antimony, etc.) would be considered as an illustration of the beneficial effect of the alloying additives on battery life. This would be a more consistent definition from a theoretical point of view. But since the behaviour of alloy electrodes has, historically, been taken as a point of reference, this approach will be continued in this paper.

Conditions that facilitate the phenomenon

It has been shown that not all operating conditions cause a manifestation of the PCL effect. The latter is exhibited only when: (i) the battery is subjected to a great number of charge/discharge cycles during its operation at a positive active-material utilization that is greater than 20% of the theoretical (Faraday) value; (ii) the battery grids are made of lead, lead–calcium, lead–calcium–tin (not a very high content of tin) and low-antimony lead alloys; (iii) the battery is flooded with a sufficient amount of H_2SO_4.

From all these criteria, it follows that the PCL phenomena are most strongly manifested in industrial batteries, i.e., traction (electric vehicle) and load-levelling batteries that are used as sources of energy and power for a considerably long service life. In this case, the PCL effect may be characterized by determining experimentally the dependence of battery capacity at high active-mass utilization on the number of charge/discharge cycles.

Batteries with lead–calcium and low-antimony lead grids have an important advantage, they require little or no maintenance. To capitalize on this benefit, it is essential to find methods for suppressing PCL phenomena in such batteries. This has been a prime target for lead/acid battery scientists and technologists during the past few years.

Models to explain premature capacity loss phenomena

For more that twenty years, numerous experimental investigations have been performed and have yielded results that have given rise to different explanations of the PCL effect. The conclusions can be divided in two groups.

Group I models

During charge/discharge cycling, the phase composition and structure of the corrosion layer (CL) are changed in such a way that the positive active material (PAM) is electrically isolated from the plate current-collector (i.e. the grid). This isolation may be due to the formation of $PbSO_4$ [3–7] and/or PbO [8–16] sublayers, or to cracking of the CL itself [13–17]. In this way, though the positive active mass is capable of current generation, the associated electrochemical processes are blocked by the changes in the CL.

Group II models

During charge/discharge cycling, both the structure and the nature of the PAM undergo changes that cause considerable parts of the PAM to be excluded from the current-generation process. The changes in the PAM are related to: (i) conversion of the agglomerate structure into a crystalline form; (ii) increase in size of the PbO_2 crystals, which impedes the contact between them [17–19]; (iii) phenomena that proceed at the interface between the crystals [20]. Other explanations are associated with changes in the electrochemical properties of PbO_2. In particular, the absence of hydrogen in the structure of the PAM results in a loss of electrochemical activity of PbO_2 and, hence, of capacity [21–23]. Changes in the ratio between the α and β modifications of PbO_2 on cycling have also been suggested as a possible cause of the PCL effect [24, 25]. More recently, it has been established that both the PAM and the CL have a gel–crystal structure. The gel zones have the lowest conductivity. The latter depends on the concentration in the gel zones of polymer chains. It has been suggested [26] that the phenomena that proceed in the gel zones of the CL/PAM interface lead to PCL.

Surveys on the above models for premature capacity loss are presented in refs. 25 and 26.

Localization of phenomena that promote premature capacity loss in the plate structure

The existence of such a diversity of models for the PCL effect requires experimental investigation to localize the sites at which this phenomenon occurs. To achieve this aim, model plates have been prepared with lead and Pb–4.5wt.%Sb subgrids that are attached to one another with epoxy resin. The design of these plates is presented in Fig. 2 [27, 28]. Each of the subgrids is a separate current-collector through which cycling of the plate may be conducted. The cycling was performed with deep discharges, namely 100% DOD at 47% utilization of PAM. In other words, the plates were operated under conditions that facilitated strongly the PCL effect.

Figure 3 presents the capacity/cycles curves for cells assembled with one positive plate (with lead and Pb–4.5wt.%Sb subgrids) and two negative plates. Cycling of cells was performed: (i) simultaneously, i.e., one of the cells was cycled through the lead subgrid and the other through the Pb–Sb one; (ii) consecutively, i.e., one cell was cycled through the lead subgrid first and then through the Pb–Sb counterpart, while the other cell was cycled through the Pb–Sb subgrid first, and after 12 cycles, through the lead subgrid.

The results presented in Fig. 3(a) show that, during the first few cycles, both cells have the same capacity. This suggests that each of the subgrids is sufficiently branched and capable of delivering the current to every point in the PAM. When

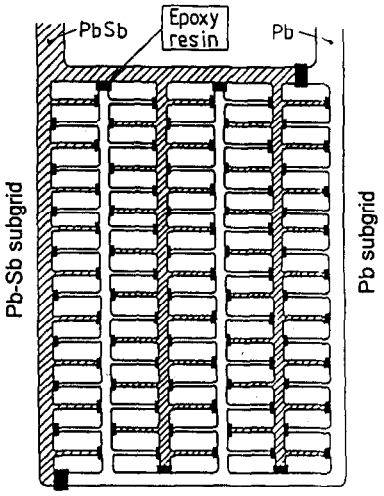

Fig. 2. Design of positive grid with lead and lead–antimony subgrids [27, 28].

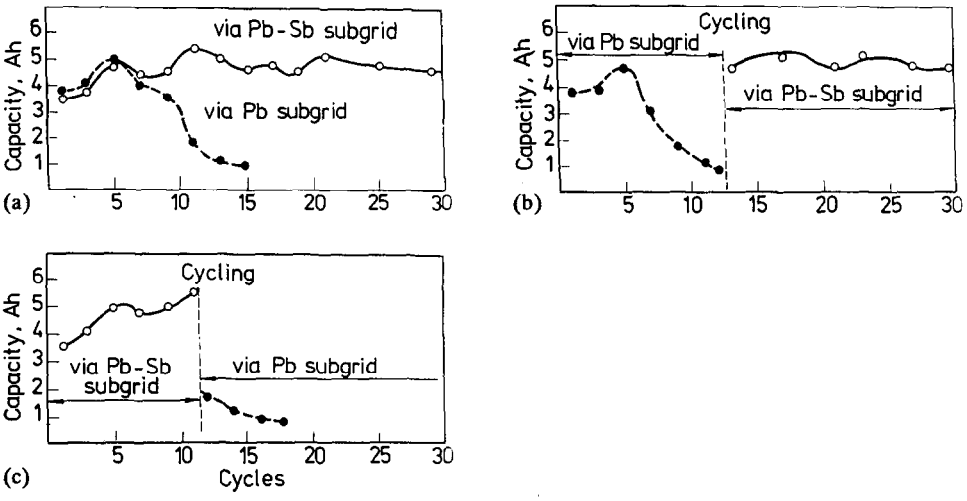

Fig. 3. Capacity changes on cycling of positive plate: (a) through lead or lead–antimony subgrids; (b) first through lead subgrid, then through lead–antimony subgrid; (c) first through lead–antimony subgrid and then through lead subgrid [28].

cycling is performed through the lead subgrid, the life of the battery is limited to 12 cycles. When a Pb–Sb subgrid is used, however, the plate preserves its capacity for more than twice as many cycles. Therefore, when the grid is made from pure lead, the capacity is determined by the properties of both the CL and its interfaces with the metal and the PAM. The same conclusion was reached when the discharge was conducted consecutively, see Fig. 3(b), (c).

The properties of the CL, and of its interfaces, depend strongly on the alloying additives to the grid alloy (in this case, antimony). Note, alloying additives will be called 'dopants' when their effects on the properties of the CL are discussed. Antimony

is responsible for those properties of the CL that do not allow it to limit the discharge of the active mass so that, the latter exhibits its full capacity.

Finally, the results with double subgrids indicate that the PbO_2 active mass is 'healthy', although on discharge through the lead subgrid, the plate has reached the end of its cycle life. If cycling is continued through the Pb–Sb subgrid, the same PbO_2 active mass exhibits its full capacity for many more cycles.

Structure of corrosion layer and positive active mass

Corrosion layer

Figure 4 presents a scheme for the structure of the CL. It suggests that, irrespective of whether it is formed on a Pb–Ca or a Pb–Sb grid, the CL consists of the following two sublayers.

(i) A dense (inner) sublayer that is fixed to the grid. The thickness of this sublayer may reach 10 to 20 μm. It comprises mainly lead oxides, i.e., PbO or PbO_n ($n \geqslant 1.5$). No $PbSO_4$ is formed in this sublayer. The sulfuric acid solution reaches only its interface with the porous sublayer.

(ii) A porous (outer) sublayer that is in contact with the electrolyte and the skeleton of the PAM. The porous sublayer consists of PbO_n and PbO_2. This sublayer takes part in the charge/discharge reactions. During discharge and self-discharge, $PbSO_4$ may be formed in the sublayer, which is then oxidized to PbO_2.

The active material of an automotive plate has a surface area of 500 to 700 m^2. The surface area of the grid is of the order of 30 to 60 cm^2. The current generated as a result of the electrochemical reaction on 700 m^2 area is concentrated in the positive active mass near the ribs of the grid, and passes through the CL and the 60 cm^2 grid surface. This makes the structure of the CL, and of its interface with the PAM, the most critical elements in the whole positive plate.

Positive active material and corrosion layer: gel–crystal structure and electric conductivity

Through observations with transmission electron microscopy (TEM) and measurements of the amount of bonded water, it has been established that both the PAM

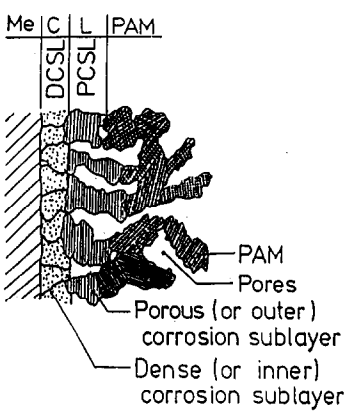

Fig. 4. Schematic representation of structure of corrosion layer.

[29, 30] and the CL [31] consist of crystal zones with α- and β-PbO_2 structures, and with hydrated (gel) zones. The latter are built of hydrated linear polymer chains that have both electron and proton conductivity, i.e.,

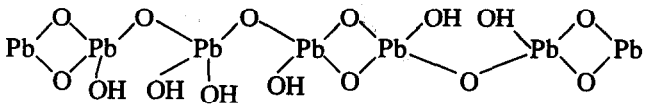

Electrons and protons move along the polymer chains. The gel zones connect the crystal zones and thus create electron and proton conductivity in the PAM. Gel zones are structural elements that have higher resistance than the crystal zones. Their resistance depends on the concentration of polymer chains in the gel and the connections between them.

As the distance between the lead ions in the polymer chains is fixed, the transfer of electrons from one lead ion to another is associated with overcoming a small potential barrier. The distances between the crystal zones are considerably larger than the length of the polymer chains. Hence, electrons have to pass through many polymer chains in order to travel from one crystal zone to another ('bridge-island conductivity'). Thus, for the movement of electrons through the gel zones, the potential barrier between two polymer chains is critical. This barrier depends on: (i) gel density: with increase in the gel density, the distances between the polymer chains are reduced and, thus, the probability for electron transfer from one chain to the other is increased;

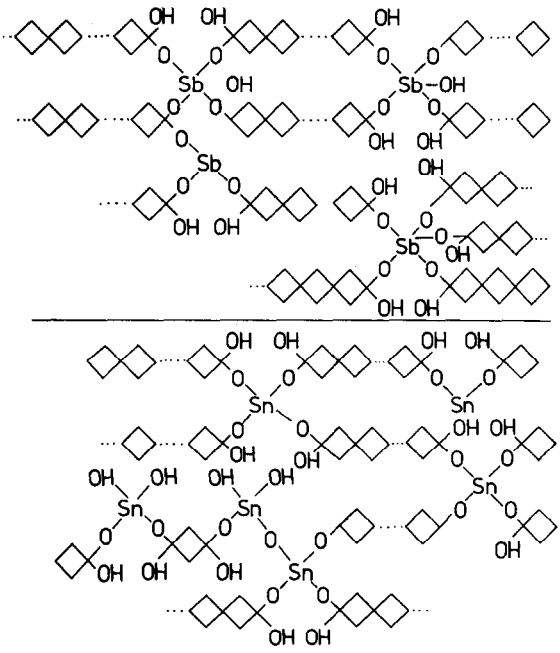

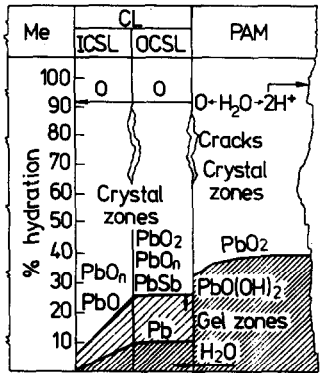

Fig. 5. Scheme for connections between hydrated polymer chains in gel zones, through antimony and tin ions, into an integral network with electron and proton conductivity [30].

Fig. 6. A model of the distribution of gel and crystal zones in the corrosion layer and the PAM. ICSL: inner corrosion sublayer; OCSL: outer corrosion sublayer.

(ii) dopants in the gel zones, i.e., ions which form chemical links between the polymer chains; by this action, the distances between the chains are fixed and a network is formed that prevents dissolution of the gel zones.

Dopant ions take part in the transfer of electrons from one polymer chain to another and, thereby, increase the conductivity of the gel zones. This is presented schematically in Fig. 5 [30]. Antimony and tin ions have high affinity towards water. Polymer chains, on their part, are hydrated. Therefore, antimony and tin form a polymer network. It is useful to call these dopants 'binders'. In the absence of a binder, the polymer network exhibits high conductivity only when there is a high density of the polymer chains in the gel. With decreasing PAM density, the conductivity of gel zones declines. This takes place during cycling of the plates. Such sensitivity of the conductivity of the gel without binder on the density of PAM is one factor that promotes PCL. It is to be expected that the layers near the grid members will be most sensitive to changes in the PAM density. Fortunately, these regions are saturated with ions of the binder; the ions are formed as a result of oxidation and subsequent leaching out of the additives in the grid alloy.

A model for the distribution of gel and crystal zones from the grid, through the CL to the active mass is presented in Fig. 6. This model takes into account the formation of cracks in the CL on battery cycling. Such cracks will affect the current transfer through the CL [13–17]. The interface metal (Me)/inner corrosion sublayer is used as an ordinate along which the degrees of hydration (in %) of the separate structural elements of the plate are presented. In general, the outer corrosion sublayer is hydrated. In pure-lead electrodes, the degree of hydration is about 10% [31], while in Pb-Sb counterparts it varies between 15 and 25%, as determined by the antimony content in the grid alloy [32]. There is 30 to 35% hydration of the PAM [33].

Formation and growth of the corrosion layer

In principle, there are two different groups of conditions under which the CL on the anodic grid is formed. These conditions result in different compositions of the CL namely:

(i) Corrosion layer induced by plate manufacture ('technological' type): formed under the technological conditions of positive-plate production and associated with the formation of PbO_n and basic sulfates during pasting and curing of the plates, and oxidation of these products during formation of the active mass;

(ii) Corrosion layer induced by battery service ('operational' type): formed during battery operation as a result of oxygen diffusion through the CL to the grid.

Formation of technological type of corrosion layer during plate curing

This layer is formed during casting of the grids, pasting of the plates and, most intensively, during plate curing. Curing is conducted at high humidity, and at either low temperature (40 to 65 °C) or high temperature (above 70 °C). The duration of the process is from 24 to 72 h. These conditions are the most conducive for oxidation of the metal to PbO. The resulting oxide film connects the metal with the skeleton of the cured paste.

Rand and Lam [34] studied the influence of the curing conditions on the capacity/cycle-life curve of positive battery plates. The plates under investigation were produced with low-antimony grids and 3BS pastes and were subjected to: (i) low-temperature curing, as a result of which the 3BS phase was preserved; (ii) high-temperature

conventional curing; (iii) advanced high-temperature curing. When the last two curing procedures were applied, the 3BS pastes were converted into 4BS material. Figure 7 presents the capacity as a function of cycle number during operation under the JIS 5361 test. It can be seen that the advanced high-temperature curing process improves substantially the life of the batteries. Similar results have also been obtained in the author's laboratory.

This effect of the curing procedure may be due to: (i) improvement of the skeleton structure of PAM when the 3BS paste is converted to a 4BS counterpart; (ii) formation of an appropriate structure and composition for the CL. In order to eliminate the role of one of the above factors, investigations were conducted [35] in the author's laboratories of the capacity/cycle-life relationship (at 100% DOD) for plates with low-antimony grids, 3BS and 4BS pastes, and high-temperature curing. To block the process of conversion of the 3BS paste to 4BS material during the high-temperature curing, 0.1 wt.% of sodium lignosulfonate expander was added to the paste. This material inhibits the formation of the 4BS phase [36]. Figure 8 presents the capacity/cycle-life curves for the above batteries. The plates prepared with 4BS pastes and cured at

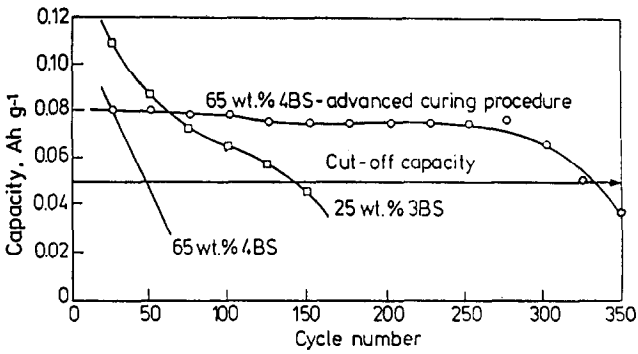

Fig. 7. Capacity performance. Test was conducted according to the JIS 5361 standard. Positive plates produced with 3BS pastes. On low-temperature curing, skeleton of cured paste is built of 3BS. On high-temperature curing, cured paste consists of 4BS crystals formed during curing [34].

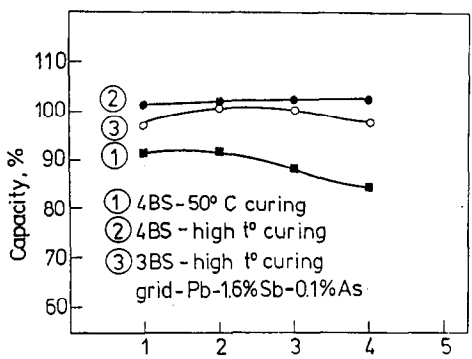

Fig. 8. Capacity/cycle curves for batteries operated at 50% utilization of active mass. Positive plates were produced with 3BS and 4BS pastes, and subjected to curing under different conditions. Cycles, 100% DOD; $i_d = 0.05\ C_{20}$ A.

65 °C have a capacity of 91%. If such plates are subjected to high-temperature curing, their capacity is increased to 103%. The plates pasted with 3BS pastes and cured at 90 °C also exhibit a capacity higher than 100%. This means that the beneficial effect of high-temperature curing is mainly due to processes that occur at the grid/past interface and is less dependent on the composition of the paste.

A comparison between curves 2 and 3 in Fig. 8 shows that plates prepared with 4BS pastes exhibit a stable capacity, while the capacity of the plates prepared with 3BS pastes begins to decline after the third cycle. This is a clear illustration of the advantages of 4BS pastes.

A determination was made of the corrosion rate (i.e., formation of PbO) as a result of the oxidation of Pb–1.6 wt.%Sb–0.1 wt.%As grids that were prepared with 1.5 mm 4BS pastes on curing for 75 h at 45 °C and 48 h at 90 °C. The data obtained are presented in Table 1. High-temperature curing leads to the formation of a thicker CL of PbO. This ensures a stable contact between the skeleton of the cured paste and the grid.

During formation of the active mass, metasomatic processes occur and the matrix of the CL/cured-paste interface is passed on to the structure of the CL/PAM interface.

Growth of corrosion layer during battery operation

During battery operation, the anodic oxidation of the lead grid to PbO_2 in H_2SO_4 solution proceeds in three stages [37], namely:

$$Pb \xrightarrow{V_1} PbO \qquad \text{(reaction of corrosion)} \tag{1}$$

$$PbO \xrightarrow{V_2} PbO_n \qquad (1<n<2) \tag{2}$$

$$PbO_n \xrightarrow{V_3} PbO_2 \tag{3}$$

These reactions reflect the oxidation of lead, PbO and PbO_n by oxygen that has diffused into the CL. The reactions proceed at different rates, i.e., V_1, V_2 and V_3. Depending on the ratio between the values of these rates, CLs with different phase compositions are formed. Thus, when $V_1 > V_2$, a PbO layer is produced at the metal surface. The electrode system is of the type $Pb/PbO/PbO_n/PbO_2$. As PbO has high electric resistance, this electrode is passivated. When $V_1 < V_2$, only PbO_n and PbO_2 are formed in the CL. The positive plate of the lead/acid battery is such a system.

It has been established [32] that antimony acts as an electrocatalyst for the oxidation reaction of PbO to PbO_n. A similar effect has been observed with tin [9] and bismuth [38]. The stoichiometric coefficient of the CL is 1.6 to 1.85 and 1.4 to 1.65 for lead–antimony [39] and lead–arsenic [40] electrode, respectively. It is known that when the stoichiometric coefficient of lead oxides reaches a value 1.4 to 1.5, their specific electroconductivity becomes equal to that of PbO_2 [41].

TABLE 1

Corrosion rates of low-antimony electrodes at low- and high-temperature curing

Curing	Weight loss (10^{-5} g h^{-1} cm^{-2})
45 °C, 72 h	1.3
90 °C, 48 h	5.3

Interaction of corrosion layer with H_2SO_4

Reaction of sulfation

PbO_n may be treated as a mixed oxide that consists of PbO and PbO_2. When the H_2SO_4 solution reaches the outer corrosion sublayer, a reaction of disproportionation and sulfation commences, i.e.:

$$PbO_n + H_2SO_4 \longrightarrow kPbO_2 + qPbSO_4 \quad (4)$$

The formation of PbO_2 in the CL has a beneficial effect on the performance of the plate. Lead sulfate is a dielectric and also reduces the cross section of the area through which the electric current passes between the PAM and the plate grid. Hence, eqn. (4) should be slowed down or suppressed.

It has been established [42] that the process of sulfation starts at the interface between the outer corrosion sublayer and the PAM, and then proceeds inwards in the layer until it reaches the surface of the inner corrosion sublayer.

The quantity of $PbSO_4$ in the CL depends, first, on the concentration of the H_2SO_4 solution, and second, on the content of the alloying additives in the grid alloy. Thus, sulfation of the CL on lead–calcium grids begins much earlier during the plate discharge than that of the CL formed on lead–antimony grids [42]. Both the past density and the thickness of the plate also influence the sulfation process of the CL [42].

Influence of H_2SO_4 concentration on capacity during cycling

Nakayama *et al.* [43, 44] and Tsubota *et al.* [45] have established that the capacity curve on cycling depends on the amount of H_2SO_4. Figure 9 [45] presents the changes in capacity of batteries with lead–calcium–tin grids on cycling: first, in flooded electrolyte, then in starved electrolyte, and again in flooded electrolyte. The experimental data show that when the amount of H_2SO_4 decreases, the battery capacity increases, and vice versa. Samples taken from the CL and subjected to microprobe analysis revealed that, when cycling is performed in starved electrolyte, the resulting CL contains small

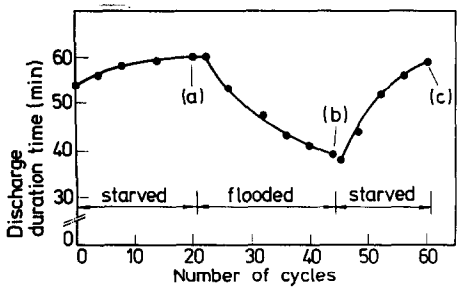

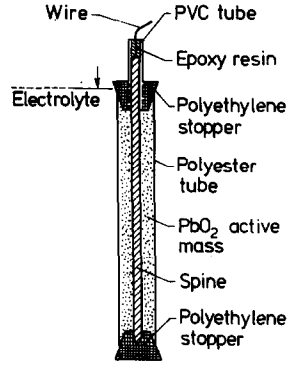

Fig. 9. Dependence of capacity/cycle curve on changes in H_2SO_4 content in cell [45]. Cycling conditions: discharge (20 A, 1.70 V); charge (5 A, 135%); temperature (40 °C). Electrolyte: 1.30 sp. gr., 20 °C.

Fig. 10. Schematic of a tubular powder electrode [46].

amounts of $PbSO_4$. By contrast, under flooded conditions, large amounts of $PbSO_4$ are contained in the CL. The information presented in Fig. 9 indicates that sulfation is a reversible process.

It has been established [7] that on deep-discharge cycling of batteries with lead–calcium–tin grids, the battery capacity decreases almost linearly with the increase in H_2SO_4 concentration from 1.1 to 1.2 sp. gr.

Influence of properties of CL/PAM interface on capacity

To investigate the influence of properties of the CL/PAM interface on plate performance, special tubular powder electrodes were developed [46]. The design is shown in Fig. 10. A woven polyester tube of a definite volume, with a spine in the centre, was filled with charged PAM powder. PbO_2 particles are known to have hydrated surface. Hence, the particles come into contact with one another, and with the spine, through their gel zones. Such model electrodes were inserted into H_2SO_4 solution and subjected to cycling. During the first few cycles, the capacity of the electrode is determined by the number of particles that are in electronic contact with the spine. Thus, the capacity may be regarded as an indirect measure of the conductivity of the gel zones. On cycling, the individual particles are interconnected into a skeleton and, thereby, restore the structure of the PAM. Such electrodes have been used to investigate the properties of the CL/PAM interface.

The effect of $PbSO_4$ content in the CL on building the electrode structure was investigated using the above electrode. First, the electrode spines, without PAM, were subjected to cycling (about 20 cycles) in H_2SO_4 solution to allow the formation of a CL that comprised two sublayers. After charge, the CL on three electrodes was discharged to 50%, and on another three electrodes to 100%. A final set of three electrodes was kept in a fully charged state. The spines were placed in tubes that were then filled with charged, powdered, PbO_2 active material. Figure 11 presents the results from cycling the tubular electrodes with Pb–2 wt.%Sb spines and a PAM density of 4.15 or 3.80 g cm^{-3} [47]. The difference between the electrodes with charged and discharged CLs is most significant during the first four cycles. After that, the variation in the capacities of electrodes with spines discharged 50 and 100% is substantially reduced.

Comparison of the specific capacities of electrodes with a PAM density of 3.80 or 4.15 g cm^{-3} demonstrates clearly that the PAM density exerts a stronger influence on the specific capacity than does the content of $PbSO_4$ in the CL. Increase in the

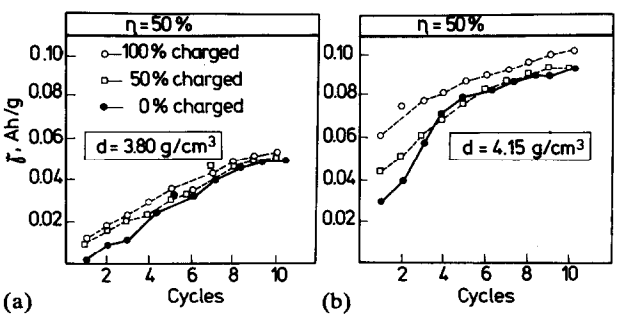

Fig. 11. Dependence of the specific capacity (γ) on number of cycles for tubular powder electrodes with 0, 50 or 100% discharged corrosion layer. Pb–2wt.%Sb spine alloy. Each curve represents data that is the average for three electrodes.

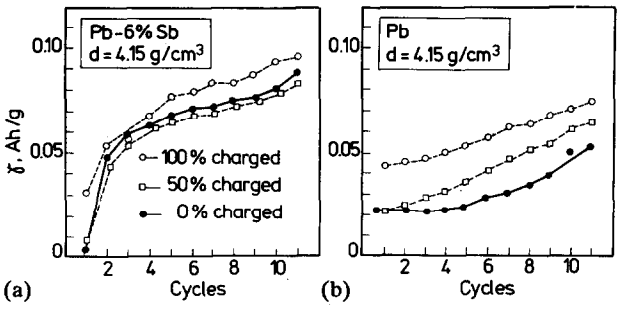

Fig. 12. Dependence of the specific capacity (γ) on number of cycles for tubular powder electrodes with 0, 50 or 100% discharged corrosion layer. Pure lead or Pb–6wt.%Sb spines. Each curve represents data that is the average for three electrodes.

PAM density leads to an increase in the number of PbO_2 particles that touch the CL. This facilitates the formation of uninterrupted gel zones between the particles and, consequently, the electrode capacity rises. The previously formed $PbSO_4$ is oxidized to PbO_2 and, thus, the structure of the electrode is built.

Figure 12 presents the dependence of the specific capacity on the number of cycles for tubular electrodes with a PAM density of 4.15 g cm^{-3} and spines made from pure lead or Pb–6 wt.%Sb alloy [47]. Electrodes with antimonial spines 'remember' only one cycle, i.e., that their CL has been discharged and that $PbSO_4$ has been formed within it. The effect of antimony on the formation of the electrode structure (i.e., CL/PAM interface and PAM skeleton) is much stronger than the electrode passivation under the action of $PbSO_4$ in the CL.

Electrodes with pure-lead spines are more sensitive to the content of $PbSO_4$ in the CL (Fig. 12(b)). They 'remember' even the degree of discharge of the CL. The specific capacity of electrodes with a 100% discharged CL is lower than that of electrodes whose CL has been discharged down to 50%.

According to the gel–crystal theory, the density of polymer chains in the CL/PAM interface on lead electrodes determines the electric conductivity of the contact. The smaller the distance between the polymer chains in the gel zones at the contact area, the higher is the conductivity. With introduction of antimony ions into the gel zones, the polymer chains are interconnected into a network and the transfer of electrons from the CL to the PAM (and vice versa) is greatly facilitated. That is why $PbSO_4$ formed preferentially in the CL is very difficult to oxidize in the case of lead electrodes, but not for electrodes with lead–antimony spines. Thus, the gel–crystal nature of the CL/PAM interface determines the intrinsic properties of this contact.

Role of plate design on CL/PAM contact during battery operation

The presence of gel zones in the PAM structure creates a dynamic structural element in the plate that can respond to the volume pulsation that occurs in the structure of the PAM and the CL during charge/discharge cycling. This feature lessens the tendency for the structures to disintegrate. In other words, the gel zones dissipate the imposed mechanical energy and allow the plate volume to increase without destruction of the active-material skeleton.

Takahashi *et al.* [48] have determined the changes in capacity, electrical resistance and thickness of the positive plate on cycling, when a force of 0.2 or 1.0 kg cm^{-2} is

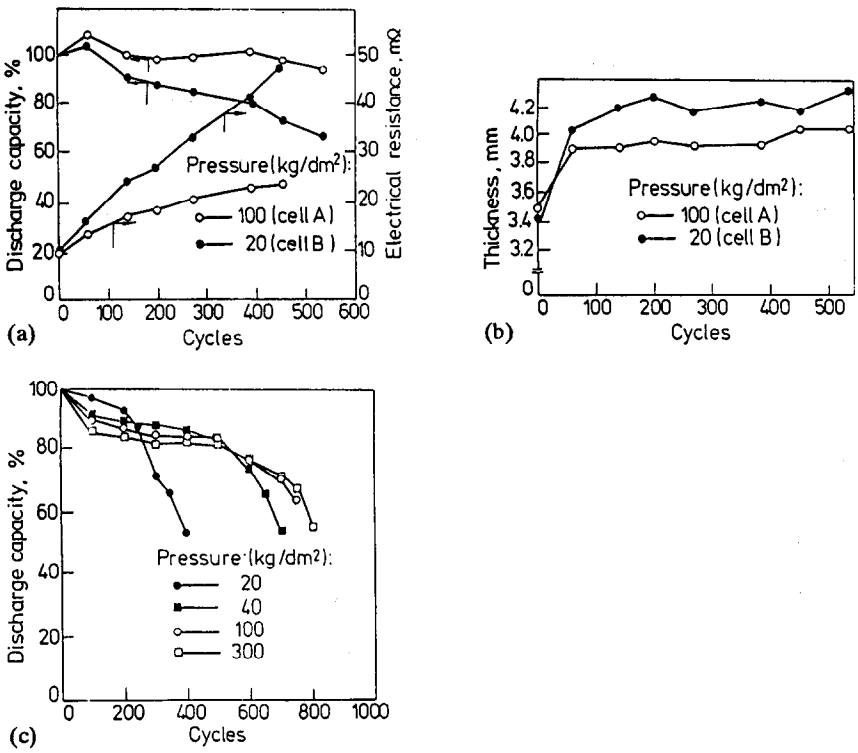

Fig. 13. (a) Changes in capacity and electric resistance during cycling of cells under pressure of 100 or 20 kg dm^{-2}; (b) dependence of plate thickness on cycle number for cells under pressure of 100 or 20 kg dm^{-2}; (c) dependence of capacity on cycle number for cells under different pressures [48].

applied to the cell (Fig. 13). Cells under high pressure exhibit smaller increases in thickness and hence smaller decreases in density of the gel zones at the CL/PAM interface. This gives rise to lower ohmic resistance and higher capacity. Restriction of the changes in plate structure, (including that of the interface CL/PAM) for a longer period will result in a longer battery life, i.e., the phenomena that cause PCL are suppressed.

Conclusions

The PCL effect is due to phenomena that occur in the CL at its interface with the PAM. These phenomena are thought to be related to a decrease in the density of the gel zones on cycling and a concomitant increase in electrical resistance. These are intrinsic properties of the interface and are determined by the gel–crystal structure of the PAM and the CL.

Through the introduction of appropriate additives (antimony, tin, etc.), that connect the polymer chains of lead dioxide into a network, the PCL effect may be suppressed. Additives, apart from playing the role of 'binders', should increase the hydrated part

of the oxides in the interface. This would allow the latter to release the inner mechanical stresses built up as a result of plate-volume pulsation during cycling.

The application of a certain, though not very high, pressure on the plates maintains a high concentration of polymer chains in the gel zones at the CL/PAM interface during cycling, and thus ensures high conductivity of the interface. This makes it possible to reduce the content of dopants in the alloy to a degree that does not enhance the decomposition of water. Therefore, a proper combination of the type and the quantity of dopants used, the PAM density, and the pressure exerted on the plate will maintain high conductivity of the gel zones at the CL/PAM interface and, accordingly, will suppress the phenomena that cause PCL.

References

1 E.E. Schumacher and G.S. Phipps, *Trans. Electrochem. Soc., 68* (1935) 309–316.
2 K. Fuchida, K. Oxada, S. Hattori, M. Kono, M. Yamane, T. Takayama, J. Yamashita and J. Nakayama, *ILZRO Project LE-276, Rep. Nos. 7 and 8,* ILZRO, Research Triangle Park, NC, USA, 1982.
3 S. Tudor, A. Weisstuch and S.H. Dowang, *Electrochem. Technol., 3* (1965) 90–94; *4* (1966) 406–411; *5* (1967) 21–26.
4 J.L. Weininger and E.G. Siwek, *J. Electrochem. Soc., 123* (1976) 602–606.
5 D. Barrett, M.T. Frost, J.A. Hamilton, K. Harris, I.R. Harrowfield, J.F. Moresby and D.A.J. Rand, *J. Electroanal. Chem., 118* (1981) 131–155.
6 S. Hattori, N. Yamashita, M. Kono, M. Yamane, M. Nakashima and J. Yamashita, *ILZRO Projects LE-253 and LA-276, Ann. Rep. 1978 and 1979,* ILZRO, Research Triangle Park, NC, USA.
7 H. Nakashima and S. Hattori, *Proc. Pb80 Int. Lead Conf., Madrid, Spain, 1980,* pp. 86–97.
8 H.K. Giess, in K.R. Bullock and D. Pavlov (eds.), *Proc. Symp. Advances in Lead-Acid Batteries,* Vol. 84-14, The Electrochemical Society, Pennington, NJ, USA, 1984, pp. 241–251.
9 D. Pavlov, B. Monahov, M. Maja and N. Penazzi, *J. Electrochem. Soc., 136* (1989) 27–33.
10 J. Garche, *J. Power Sources, 30* (1990) 47–54.
11 H. Doring, J. Garche, H. Dietz and K. Wiesener, *J. Power Sources, 30* (1990) 41–46.
12 R.F. Nelson and D.M. Wisdom, *J. Power Sources, 33* (1991) 163–185.
13 D.L. Douglas and G.W. Mao, in D.H. Collins (ed.), *Power Sources 4, Research and Development in Non-mechanical Electrical Power Sources,* Oriel Press, Newcastle-upon-Tyne, 1973, pp. 561–567.
14 B.K. Mahato, *J. Electrochem. Soc., 126* (1979) 365–370.
15 S. Hattori, M. Yamaura, M. Kono, M. Yamane, H. Nakashima, J. Yamashita and J. Nakayama, *ILZRO Project LE-276, Rep. No. 5,* 1980, ILZRO, Research Triangle Park, NC, USA.
16 D.C. Constable, J.K. Gardner, J.A. Hamilton, K. Harris, R.J. Hill, D.A.J. Rand, S. Swan and L.B. Zalcman, *ILZRO Project LE-290, Ann. Rep. 1982; J. Power Sources, 23* (1988) 257–277.
17 J. Burbank, *J. Electrochem. Soc., 116* (1964) 765–770; *111* (1964) 1112–1118.
18 E.J. Ritchi and J. Burbank, *J. Electrochem. Soc., 116* (1969) 125–133; *117* (1970) 299–305.
19 D. Pavlov, E. Bashtavelova and V. Iliev, in K.R. Bullock and D. Pavlov (eds.), *Proc. Symp. Advances in Lead-Acid Batteries,* Vol. 81–14, The Electrochemical Society, Pennington, NJ, USA, 1984, pp. 16–32.
20 A. Winsel, E. Voss and U. Hullmeine, *J. Power Sources, 30* (1990) 209–226.
21 S.M. Caulder and A.C. Simon, *J. Electrochem. Soc., 121* (1974) 1546–1552.
22 J.P. Pohl and H. Rickert, in D.H. Collins (ed.), *Power Sources 5,* Academic Press, London, 1975, pp. 15–21.
23 R.J. Hill and I.C. Madsen, *J. Electrochem. Soc., 131* (1984) 1486–1491.
24 V.H. Dodson, *J. Electrochem. Soc., 108* (1961) 406–412.
25 A.F. Hollenkamp, *J. Power Sources, 36* (1991) 567–585.

26 D. Pavlov, *J. Power Sources, 42* (1993) 345–363.
27 M. Dimitrov, *Proc. Int. Conf. on Lead/Acid Batteries, LABAT '93, St. Konstantin, Varna, Bulgaria, June 7–11, 1993,* pp. 33–34.
28 M. Dimitrov and D. Pavlov, *J. Power Sources, 46* (1993) 203–210.
29 D. Pavlov, *J. Electrochem. Soc., 139* (1992) 3075–3080.
30 D. Pavlov, *J. Power Sources, 46* (1993) 171–190.
31 B. Monahov and D. Pavlov, *J. Appl. Electrochem.*, in press.
32 B. Monahov and D. Pavlov, *Proc. Int. Conf. on Lead/Acid Batteries, LABAT '93, St. Konstantin, Varna, Bulgaria, June 7–11, 1993,* pp. 61–65.
33 D. Pavlov, I. Balkanov, T. Halachev and P. Rachev, *J. Electrochem. Soc., 136* (1989) 3189.
34 D.A.J. Rand and L.T. Lam, *The Battery Man,* (Nov.) (1992) 19–23.
35 D. Pavlov, St. Ruevski and T. Rogachev, in preparation.
36 D. Pavlov and I. Iliev, *Elektrokhimiya, 12* (1975) 1735–1741.
37 D. Pavlov and T. Rogachev, *Electrochim. Acta, 23* (1978) 1237–1249.
38 M. Bojinov and D. Pavlov, *Proc. Int. Conf. on Lead/Acid Batteries, LABAT '93, St. Konstantin, Varna, Bulgaria, June 7–11, 1993,* pp. 72–76.
39 T. Rogachev, *J. Power Sources, 23* (1988) 331–344.
40 D. Pavlov and T. Rogachev, *Electrochim. Acta, 31* (1986) 241–253.
41 F. Lappe, *J. Phys. Chem. Solids, 23* (1962) 1563–1572.
42 T.G. Chang and E.M. Valeriote, *J. Electrochem. Soc., 132* (1985) 1783–1788.
43 Y. Nakayama, M. Kono and S. Hattori, *YUASA Jiho, 51* (1981) 24–38.
44 Y. Nakayama, T. Takayama and M. Kono, *YUASA Jiho, 53* (1982) 56–63.
45 M. Tsubota, S. Osumi and M. Kosai, *J. Power Sources, 33* (1991) 105–116.
46 D. Pavlov, A. Dakhouche and T. Rogachev, *J. Power Sources, 30* (1990) 117–129; *42* (1993) 71–88.
47 D. Pavlov, A. Dakhouche and T. Rogachev, in preparation.
48 K. Takahashi, M. Tsubota, K. Yonezu and K. Ando, *J. Electrochem. Soc., 130* (1983) 2144–2149.